Distributed lump kinetic modeling for slurry phase vacuum residue hydroconversion

Barbara Browning, Isabelle Pitault, Françoise Couenne, Tim Jansen, Maxime Lacroix, Pedro Alvarez, Mélaz Tayakout-Fayolle

▶ **To cite this version:**

Barbara Browning, Isabelle Pitault, Françoise Couenne, Tim Jansen, Maxime Lacroix, et al.. Distributed lump kinetic modeling for slurry phase vacuum residue hydroconversion. Chemical Engineering Journal, 2019, 377, pp.119811. 10.1016/j.cej.2018.08.197 . hal-01919533

HAL Id: hal-01919533
https://hal.science/hal-01919533

Submitted on 20 Jul 2022

HAL is a multi-disciplinary open access archive for the deposit and dissemination of scientific research documents, whether they are published or not. The documents may come from teaching and research institutions in France or abroad, or from public or private research centers.

L'archive ouverte pluridisciplinaire **HAL**, est destinée au dépôt et à la diffusion de documents scientifiques de niveau recherche, publiés ou non, émanant des établissements d'enseignement et de recherche français ou étrangers, des laboratoires publics ou privés.

Distributed under a Creative Commons Attribution - NonCommercial 4.0 International License

Version of Record: https://www.sciencedirect.com/science/article/pii/S1385894718316747
Manuscript_f78c2dcf4aae19e3cc95202e82c6a88a

Distributed Lump Kinetic Modeling for Slurry Phase Vacuum Residue Hydroconversion

Barbara Browning[a], Isabelle Pitault[a], Francoise Couenne[a], Tim Jansen[b], Maxime Lacroix[b], Pedro Alvarez[b], Mélaz Tayakout-Fayolle[a]*

[a] Univ Lyon, Université Claude Bernard Lyon 1, CNRS, LAGEP UMR 5007, 43 boulevard du 11 novembre 1918, F-69100, VILLEURBANNE, France

[b] TOTAL Research and Technology Gonfreville, Zone Industrielle du Havre, BP27, 76700 Harfleur, France

* Corresponding author

melaz.tayakout-fayolle@univ-lyon1.fr tel: +33 4 72 44 53 26

Abstract

A detailed distributed lumped kinetic model for slurry phase Vacuum Residue hydroconversion process (boiling range 525+°C) has been constructed. Simulated distillation and Gel Permeation Chromatography analysis results were combined to estimate feedstock and product compositions over the whole boiling range. The model uses 21 distributed lumps to represent the hydrocarbons, takes hydrogen consumption into account and calculates reaction rates using molar concentrations. Vapour liquid mass transfer resistances and vapour-liquid equilibrium are also accounted for. The resulting model represents the evolution of the reaction mixture physical properties well and provides a good fit with the experimental data. From estimated parameters, it is deduced that thermally activated and catalytic reactions in cascade occur simultaneously and also that material boiling above 750°C is converted in a different manner to lighter material.

Keywords: kinetic modeling; slurry phase hydroconversion; distributed lumped model; vacuum residue

© 2018 published by Elsevier. This manuscript is made available under the CC BY NC user license
https://creativecommons.org/licenses/by-nc/4.0/

1. Introduction

Oil demand is predicted to rise until 2040, particularly for use as petrochemical feedstocks and transportation fuels for trucks, aviation and shipping [1]. At the same time, an increasing proportion of the World's oil resources are in the form of unconventional and heavy crudes [2]. These contain a large fraction of residue which must be upgraded to lighter cuts to fit the demand profile. Vacuum Residue (VR), is the heaviest outlet stream from crude oil distillation. With a boiling range of 525+°C and high molecular weight, this material has high viscosity and low hydrogen to carbon ratio [3].

The earliest VR upgrading processes were via coking or visbreaking where carbon is rejected [4]. Hydrogen addition processes are more recent and are an extension of hydrocracking technologies which use heterogeneous bifunctional catalysts to simultaneously promote hydrogenation and cracking of feedstocks, such as gas oils [5]. The low diffusivity and hydrogen content of VR cause mass transfer and coking problems with traditional hydrocracking catalysts [6,7]. Slurry phase hydroconversion processes are becoming more important because they overcome this by relying on thermal cracking and using finely dispersed non-supported hydrogenation catalyst precursors, sometimes formed in-situ [8] and operating in bubble columns. Calderon and Ancheyta [9] reviewed the current literature on slurry phase reactor modelling for heavy oil hydrocracking. The equipment is typically a slurry bubble column reactor operated between 410-460°C and 100-200 bar, where the catalyst is in suspension and hydrogen is bubbled through the mixture in co- or counter-current flow.

Quitian and Ancheyta [10] recently considered kinetic models developed with residue feedstocks and slurry phase catalysts in batch reactors. For hydroconversion, it is usual to

construct a traditional lumped model with a small number of lumps based on the feedstock and liquid products. In 1997, Carbonell and Guirardello [11] constructed a slurry bubble column reactor model applied to hydroconversion of heavy oils. They used the seven lump kinetic model developed by Mosby et al. [12] and recent lumping strategies for hydroconversion are similar [13–15]. In this method, rate constants are estimated for each reaction and the number of lumps is limited by how many significant parameters can be estimated [16,17]. A wide range of calculated activation energies can be found in the literature. In general, the values are quite high, consistent with thermal reaction, particularly for the heaviest material [10, 11, 13, 14]. One drawback of traditional lumped models is that they fail to fully exploit the data which is generally in the form of distillation curves. Another downside of traditional lumped models is that the heaviest lump has no upper boiling point and covers an enormous range of components with different physical properties. The main difficulty this presents is in physical property estimation. For example, to gain sufficient detail to model viscosity conversion for thermal cracking of heavy oils, Rueda-Velasquez and Gray [18] extrapolated simulated distillation data and divided the result into multiple lumps. Distributed and continuous lumped models, such as those of Stangeland [19] and Laxaminarasimhan et al. [20] respectively were developed to overcome this problem for hydrocracking kinetics. Stangeland's model based on three parameters to describe cracking reactions forms the basis of other kinetic works [21-26]. Although the catalyst and feed effects on model parameters were discussed, Stangeland [19] did not mention the details of parameter estimation and reactor modelling. Mohanty et al. [21] provided a detailed description of thermodynamic properties for the modelling of a hydrocracking reactor using Stangeland's model. Pacheco et al. [22] improved the model by introducing two new parameters and hydrogen consumption into the mass balance closure. Similarly, Li et al. [23] developed a method to estimate the reaction stoichiometry based on the carbon balance

calculation. Later, Li and Cai [24] improved the parameter estimation using a Non-dominated Sorting Genetic Algorithm (NSGA-ii). Recently, this algorithm was also used with Stangeland's model by Harode and Ramteke [25] to optimize the production of middle distillates in a two-stage industrial hydrocracker. The works mentioned above were carried out using data from industrial units for VGO hydrocracking. As slurry hydroconversion is still a technology in development, no distributed kinetic models have been reported in the literature. Most of the kinetic models for the slurry hydroconversion of vacuum residues are based on traditional [10,13] and continuous [26] lumping approaches.

Hydroconversion rate equations can be calculated based on mass [11,14] or molar [13,27] concentrations. For hydrocracking, more kinetic models have been tested and mass concentrations are most commonly used with traditional lumped models [28]. The benefit of molar concentrations is to provide a more intrinsic kinetic model, independent of reactor type, and, indeed, these are used where possible. An example is in single event kinetics models which build up from the reactions taking place between individual molecules [29,30]. An alternative method to generating lumps from distillation curves is molecular reconstruction. In recent years, molecular-level kinetic models have been developed in order to introduce a better description of chemical species and reactions for the cracking of vacuum residues [31-35]. Klein research group (KRG) proposed a method based on attribute groups (cores, inter-core linkages, and side chains) using the bond-electron matrix to define chemical species and probability density functions (PDFs) to determinate chemical composition [31-32]. Horton et al. [33] have developed a kinetic model which calculates reaction rates directly from attributes, and not molecular concentrations, significantly reducing the number of mass balance equations to be solved. Rueda-Velasquez and Gray [34] and Oliveira et al. [35] developed similar methods using PDFs and Monte Carlo procedures to describe chemical

species, following KRG's works in the 1990's [36-38]. This kind of model has also been implemented in other refining processes. Recently, Nguyen et al. [39] used the Kinetic Modeler's Toolbox (KMT) [40] along the same principles to develop kinetic model for light gas oil hydrodesulphurization. Although molecular-level kinetic models are more sophisticated and robust than distributed lumped models, their development requires great efforts in terms of analytical techniques, which is, in some cases, a limiting aspect. High Temperature Simulated Distillation (HTSD) and Gel Permeation Chromatography (GPC) are two of the easiest analytical techniques to implement for the characterization of petroleum residues. The HTDS is quantitative but 750°C+ residue information is not available and GPC is not quantitative but all information is available. These techniques can be combined to develop a detailed distributed lumped kinetic by solving two classic difficulties: i) the acquisition of 750°C+ residue information where HTSD data is not available and ii) the estimation of the residue molar mass which evolves as high molecular weight products are consumed with processing.

The objective of this work is to construct a kinetic model for slurry phase hydroconversion which can account for the evolution of the residue molar mass and volume as the reaction progresses. A more detailed description of the physical properties is a step towards better understanding the reactivity and effect of aging on the material to be upgraded. In this article, we present an 18 parameter kinetic model with distributed lumps covering the entire VR boiling range and including four cracking reactions. This is followed by a discussion of the results and comparison with experimental data.

2. Material and methods

2.1. Experimental set-up

Hydroconversion reactions were performed in a laboratory scale (500 mL) semi-batch stirred tank reactor with reflux, condenser and online outlet stream gas phase analysis. Figure 1 gives the equipment set up. The feedstock was a Safaniya VR with 5.6 wt % sulphur content and density of 1058 $kg.m^{-3}$ at 15°C and atmospheric pressure. This was mixed with a catalyst precursor and H_2 at 150 bar upstream of the reactor. Four operating temperatures, which are reported relative to a reference temperature, T_{ref}, span a range of 30°C. For each temperature, hydroconversion reactions were carried out with 7 different reaction times (defined as t_0=0 h to t_6=6 h), including one which was stopped immediately after the heating period to give the initial composition for the kinetic model. In total, 28 experiments were performed in the campaign which forms the basis for kinetic modelling. Results were also available for a second, separate set of 30 hydroconversion experiments carried out with the same feedstock, under the same operating conditions and using an almost identical reactor set-up. The only difference being that the second reactor was smaller (250 mL) and did not include the liquid reflux stream. For each experiment, gas, H_2 and H_2S molar flow rates were measured by a Brooks instrument Quantim Series Coriolis Flow Meter and analyzed by a SRA Instrument R3000 series micro-GC using two modules PoraPLOTU (8 m x 0.32 mm ID) and OV1 (8 m x 0.15 mm ID). At the end of the reaction time, after cooling, the reactor and condenser liquids were combined for analysis. High Temperature Simulated Distillation (HTSD) analysis was carried out using an Agilent series 6890 chromatography column based on ASTM guideline D7169 [41]. Gel Permeation Chromatography (GPC) was performed using an Agilent 1200 series system. Mass balance data was accurate to ± 3% with a very small, non-quantifiable amount of sediment observed on discharging the reactor.

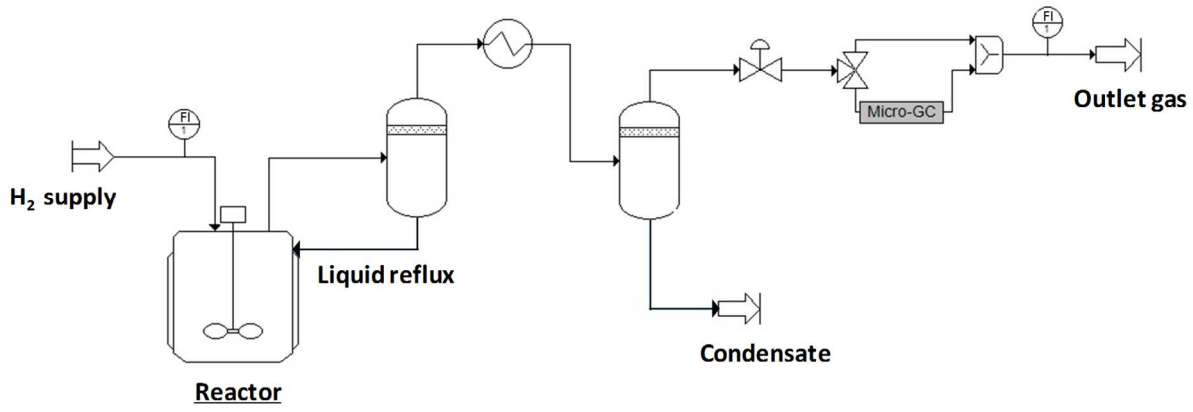

Figure 1. Process Flow Diagram of equipment set up

2.2. Experimental results and HTSD extrapolation

HTSD and online outlet gas analysis results for 28 experiments, covering a range of durations up to 6 h and at four different operating temperatures were used as the basis for kinetic model construction. HTSD and GPC analysis are available for the feedstock and for a second separate set of hydroconversion experiments. Figure 2 shows typical HTSD results for the feedstock and liquid products at high and low conversion along with the molar mass distributions (MMD) found by GPC. HTSD involves applying a linear temperature gradient to the sample to generate vapour which is analysed by GC on a nonpolar column. Results are calibrated using boiling points of normal alkanes and are quantitative. ASTM guidelines for simulated distillation methods allow analysis of heavy oils up to an atmospheric equivalent boiling point of 750°C[42]. GPC gives a MMD based on separation of components according to their hydrodynamic volume. The sample is passed through a column filled with macro-porous polymer gel. More pores are accessible to smaller molecules so these are more strongly retarded. This method is often used with polymers and the MMD is found by

calibration with polystyrene. The result is not quantitative but does allow the composition of the entire sample to be analysed. Extrapolation by the method described in Riazi [43], which uses Eq. (1), can be used to complete the HTSD data for the whole boiling range.

$$\frac{T_b - T_{b0}}{T_{b0}} = \left[\frac{A}{B} ln\left(\frac{1}{1 - x_c}\right)\right]^{\frac{1}{B}} \tag{1}$$

Since GPC data was available for the entire boiling range we established the relation given in Eq. (2) to calculate the missing part of the HTSD curves. For this, we assumed the intensity measurement on the y-axis of the GPC curves was an extensive property and therefore, proportional to mass. The GPC data was integrated, normalised and interpolated to put it into the same form as the HTSD curves with M the molar mass at each T_b data point. The parameters a, b and d were estimated from T_b and M for the boiling range to 750°C and then used to extrapolate the HTSD curves.

$$T_b = a + bM^d \tag{2}$$

Figure 3 shows that the two extrapolation methods give identical results. This is therefore a strong validation of the use of GPC analysis to extrapolate the missing part of the HTSD curve.

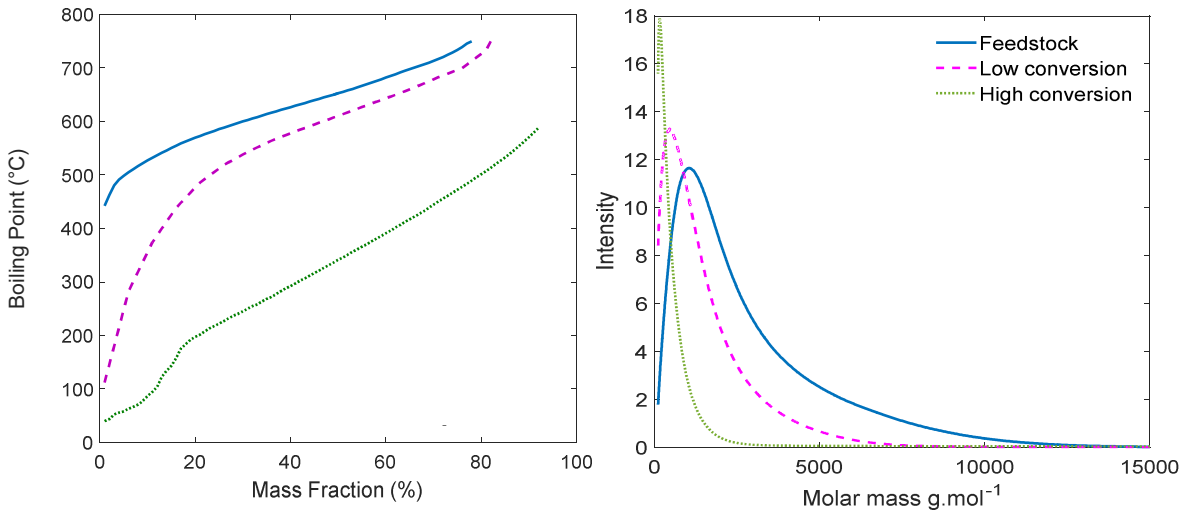

Figure 2. Typical experimental results (a) Simulated Distillation curves (b) Molar mass distribution found by Gel Permeation Chromatography. Feedstock, low conversion and high conversion products represented by solid, dashed and dotted lines respectively.

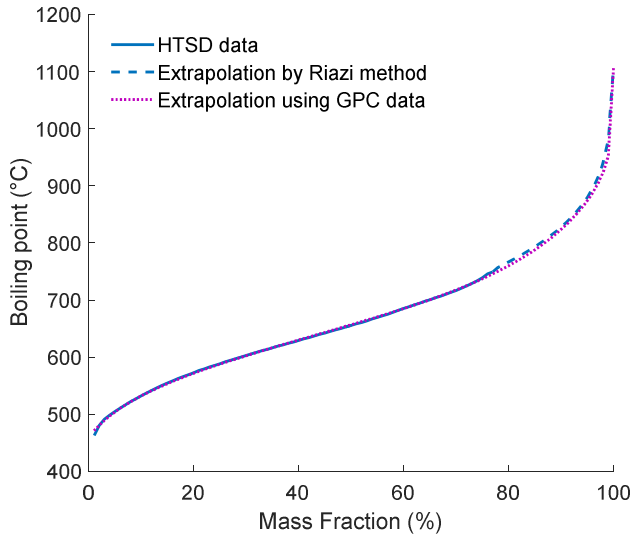

Figure 3. Extrapolated Simulated Distillation curve for feedstock

3. Model Construction

Global and component mass balances were constructed over the reactor liquid and vapour phases and for the condenser based on the following assumptions:

- Isothermal operation
- All reactions occurring in the liquid phase,
- Mass transfer limitation taken into account only between liquid and vapour phases ,
- Ideal liquid mixing,
- Perfect mixing in the condenser and reactor liquid and vapour phases,
- The vapour phase is considered an ideal gas,
- No liquid hold up in the condenser

Equilibrium constants were estimated using ProSimPlus software version 3.3 and used to perform flash calculations for reaction conditions. A simple partition coefficient based on these equilibrium constants was used to calculate the liquid reflux for the hydrocarbons returning from the condenser to the reactor. A plug flow regime was used to calculate the measurement delay caused by the tubing between the condenser outlet and the online gas analysis. The reactor model is based on the diagram given in Figure 4 with P_{op} and T_{op} the reactor operating pressure and temperature and P_c and T_c the conditions in the condenser:

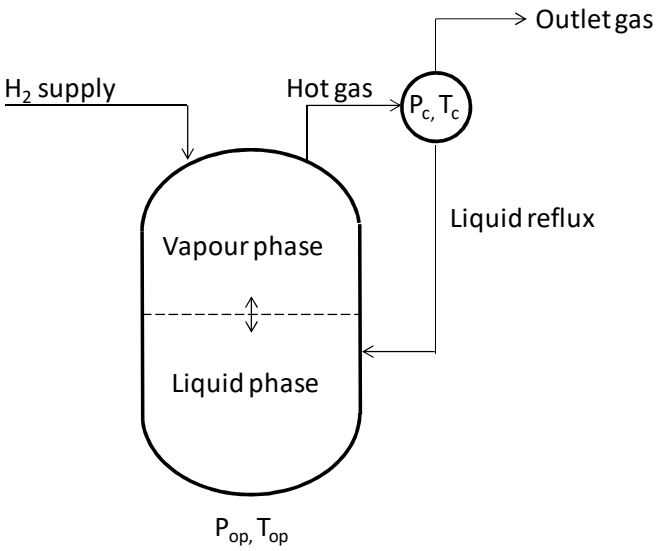

Figure 4. Diagram of reactor model

3.1 Reactor model

The material balances are calculated using molar quantities. Eq. (3) gives the component balances for the reactor liquid phase. Lumps can be either consumed or produced by reaction and the reaction rates, $\dot{n}_{i\_prod}$, are calculated using the kinetic model (see Eq.s 26 – 28). Mass transfer between the liquid and vapour phases occurs and the rates, $\dot{n}_{i\_ech}$, are found from Eq. (4), with C_i^* the equilibrium concentrations. Finally, liquid enters via the reflux stream and the rates for this, $\dot{n}_{i\_reflux}$, are determined using Eq.s (5) to (11).

$$\frac{dn_i^L}{dt} = \dot{n}_{i\_prod} + \dot{n}_{i\_ech} + \dot{n}_{i\_reflux} \tag{3}$$

$$\dot{n}_{i\_ech} = k_l a(C_i - C_i^*)V_L \tag{4}$$

Eq.s (5), (6) and (7) are the overall balances for the reactor and the balance for the reactor vapour phase components. In Eq. (7) the term $\dot{n}_{i\_H2\_supply}$ is zero for all components except

H_2. Eq. (8) is the constraint of fixed reactor volume and Eq.s (9) and (10) give the total volumes of the liquid and vapour phases based on composition and molar volume. These are all combined to give Eq. (11) with x_{i_reflux} the condensed fraction of each component. Finally, Eq. (11) can be substituted into Eq. (3) to give the mole balance, Eq. (12), with A and B given by Eq.s (13) and (14) respectively.

$$\frac{dn^L}{dt} = \sum_i \dot{n}_{i\_prod} + \sum_i \dot{n}_{i\_ech} + \dot{n}_{reflux} \tag{5}$$

$$\frac{dn^V}{dt} = \dot{n}_{H2\_supply} - \sum_i \dot{n}_{i\_ech} - \dot{n}_{hot\_gas} \tag{6}$$

$$\frac{dn_i^V}{dt} = \dot{n}_{i\_H2\_supply} - \dot{n}_{i\_ech} - \dot{n}_{i_{hot\_gas}} \tag{7}$$

$$V^L = \sum n_i^L V_{mol\_i}^L \tag{8}$$

$$V^V = V^R - V^L \tag{9}$$

$$V_{mol}^V = \frac{V^V}{n^V} \tag{10}$$

$$\dot{n}_{i\_reflux} = x_{i\_reflux}\ y_i \left(\dot{n}_{H2\_supply} - \dot{n}_{ech} + \frac{1}{V_{mol}^V} \sum \frac{dn_i^L}{dt} V_{mol\_i}^L \right)$$

(11)

$$\begin{bmatrix} \frac{dn_1^L}{dt} \\ \frac{dn_2^L}{dt} \\ \vdots \\ \frac{dn_n^L}{dt} \end{bmatrix} = [A]^{-1}[B]$$

(12)

$$[A] = \begin{bmatrix} 1 - \frac{x_{1_{reflux}}\ y_1}{V_{mol}^V} V_{mol_1}^L & -\frac{x_{1_{reflux}}\ y_1}{V_{mol}^V} V_{mol_2}^L & \cdots & -\frac{x_{1_{reflux}}\ y_1}{V_{mol}^V} V_{mol_n}^L \\ -\frac{x_{2_{reflux}}\ y_2}{V_{mol}^V} V_{mol_1}^L & 1 - \frac{x_{2_{reflux}}\ y_2}{V_{mol}^V} V_{mol_2}^L & \cdots & -\frac{x_{2_{reflux}}\ y_2}{V_{mol}^V} V_{mol_n}^L \\ \vdots & \vdots & \ddots & \vdots \\ -\frac{x_{3_{reflux}}\ y_3}{V_{mol}^V} V_{mol_1}^L & -\frac{x_{3_{reflux}}\ y_3}{V_{mol}^V} V_{mol_2}^L & \cdots & 1 - \frac{x_{3_{reflux}}\ y_3}{V_{mol}^V} V_{mol_n}^L \end{bmatrix}$$

(13)

$$[B] = \begin{bmatrix} \dot{n}_{1\_prod} + \dot{n}_{1\_ech} + x_{1\_reflux}\ y_1 \left(\dot{n}_{H2\_supply} - \dot{n}_{ech} \right) \\ \dot{n}_{2\_prod} + \dot{n}_{2\_ech} + x_{2\_reflux}\ y_2 \left(\dot{n}_{H2\_supply} - \dot{n}_{ech} \right) \\ \vdots \\ \dot{n}_{n\_prod} + \dot{n}_{n\_ech} + x_{n\_reflux}\ y_n \left(\dot{n}_{H2\_supply} - \dot{n}_{ech} \right) \end{bmatrix}$$

(14)

3.2 Kinetic model

The kinetic model was applied from t_0, the moment the reactor achieved the operating temperature. Some thermal cracking reactions occur beforehand, during reactor heating once

the reactor is above 300°C. The vapour phase initial conditions are adjusted to take the small amounts of H_2 consumed and H_2S and gas produced into account.

True boiling points were used to define traditional hydrocarbon lumps as GAS (T_b < 36°C), NAPH (36°C < T_b < 160°C), DIST (160°C < T_b < 350°C), VGO (350°C < T_b < 525°C) and RES (525°C +). The VGO and RES lumps were then subdivided into 18 boiling ranges of 35°C as follows: VGO_i with i = 1 to 5, $LRES_i$ with i = 6 to 11 and $HRES_i$ with i = 12 to 18. This fixes an upper boiling limit for the RES at 980°C. Figure 5 gives the mass distribution for the feedstock after lumping. Only three VGO lumps are shown because the feedstock does not contain VGO_1 or VGO_2. The model has two additional components which take part in reactions: H_2 and H_2S.

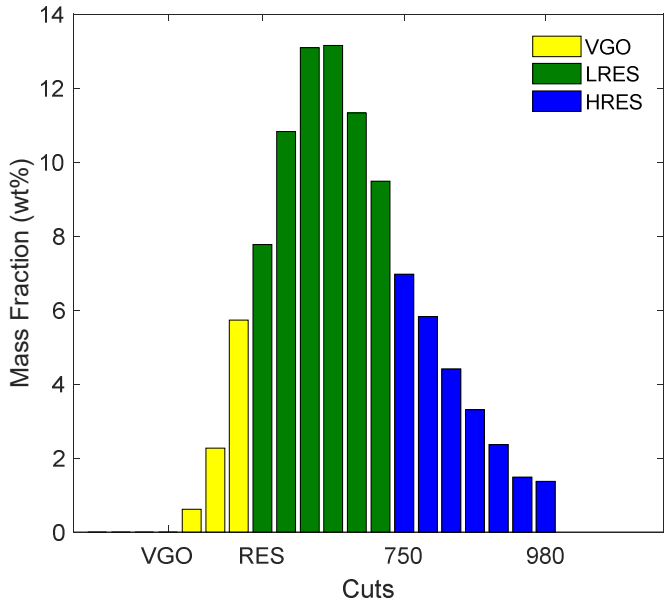

Figure 5. Mass fraction distribution of the feedstock

Molar masses and volumes are required for the model and these were estimated using ProSimPlus 3.3. The extrapolated HTSD curves and the density data are input to the simulator which represents them as pseudocomponents. The SRK equation of state and Grayson-Streed thermodynamic model were used with the TWU correlation to find the

physical properties of each pseudocomponent under reaction conditions. This was then used to estimate values for each lump used in the kinetic model. The variation over the operating temperature range of the reactor is slight and is therefore neglected. Figure 6 gives the results for all the lumps.

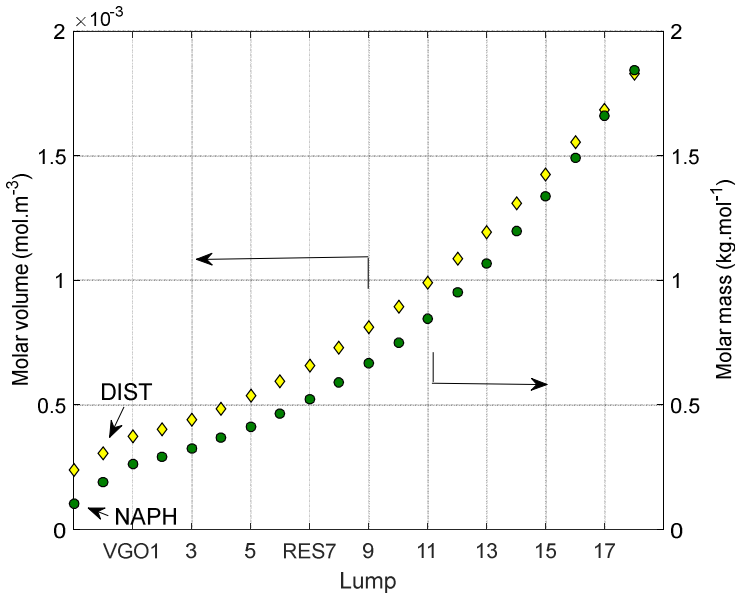

Figure 6. Calculated molar masses and molar volumes of hydrocarbon lumps

The reaction scheme is constituted by four families of hydrocracking reactions and one set of hydrodesulphurisation (HDS) reactions. For clarity, the reaction scheme is separated into diagrams for thermally activated and catalytic reactions respectively shown in Figure 7 and Figure 8. Note that around 40 different kinetic models and reaction schemes were tested and compared against the experimental data. The version presented here is that which minimizes the sum of the errors squared the individual errors around zero and centers them and the number of parameters.

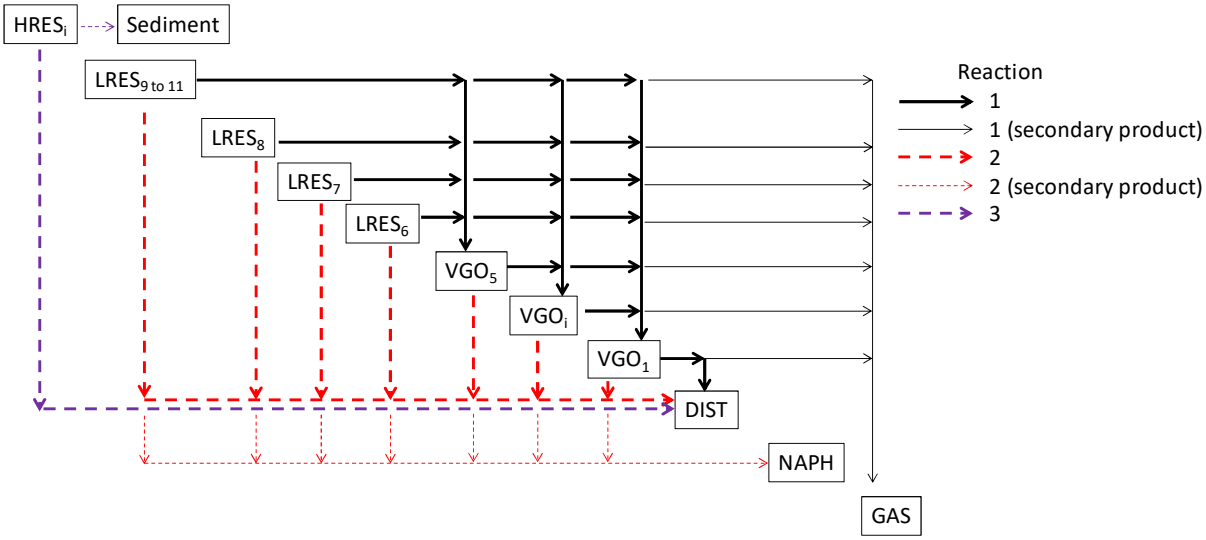

Figure 7. Reaction scheme showing thermally activated reaction sets 1, 2 and 3

All reactions consume H_2 and the hydroconversion reactions all produce lighter gas oil products. Reactions 1, 2 and 3 are defined as thermally activated. They are shown in Figure 7 and listed in Eq.s (15) to (21).

Reaction 1: (15)

$$LRES_i \rightarrow v_{1_i}\,\beta_j\,VGO_j + v_{1_{GAS}}GAS$$

with i from 6 to 11 and j from 1 to 5 and

$$\beta_j = \frac{1}{N_{VGO}} + \left(\frac{(N_{VGO}+1)}{2} - j\right)\alpha \quad (16)$$

$$VGO_i \rightarrow v_{1_i}\,\beta_j\,VGO_j + v_{1_{GAS}}GAS \quad (17)$$

with i from 2 to 5 and j from 1 to 4

$$VGO_1 \rightarrow v_{1_{VGO1}}DIST + v_{1_{GAS}}GAS \quad (18)$$

Reaction 2: (19)

$$LRES_i \rightarrow v_{2_i} DIST + v_{2_{NAPH}} NAPH$$

$$VGO_i \rightarrow v_{2_i} DIST + v_{2_{NAPH}} NAPH \quad (20)$$

Reaction 3: (21)

$$HRES_i \rightarrow v_{4_i} DIST + SEDIMENT$$

They give the same products as traditional lumping models, i.e. VGO, DIST, NAPH and GAS. So, products are mainly much lighter than parent molecules. For reaction sets 1 and 2, the stoichiometric coefficients for the hydrocarbon products, v_{r_i}, are estimated for the heaviest lump with the values for the other reacting lumps calculated proportional to their molar mass. The stoichiometric coefficients for the GAS and NAPH are calculated to complete the mass balance. The repartition coefficient for the reaction 1 VGO product, β_j, gives a linear distribution, such that the greater the value of the independent parameter, α, the more VGO_1 is produced, see Eq. (16) where N_{VGO} is the number of VGO lumps.

In reaction set 3, all HRES lumps are assumed to be converted into DIST and sediment. However, the sediment quantity is tiny and non-quantifiable and therefore neglected in the calculations. So, in the model, all the converted material becomes DIST and no stoichiometric coefficient is estimated.

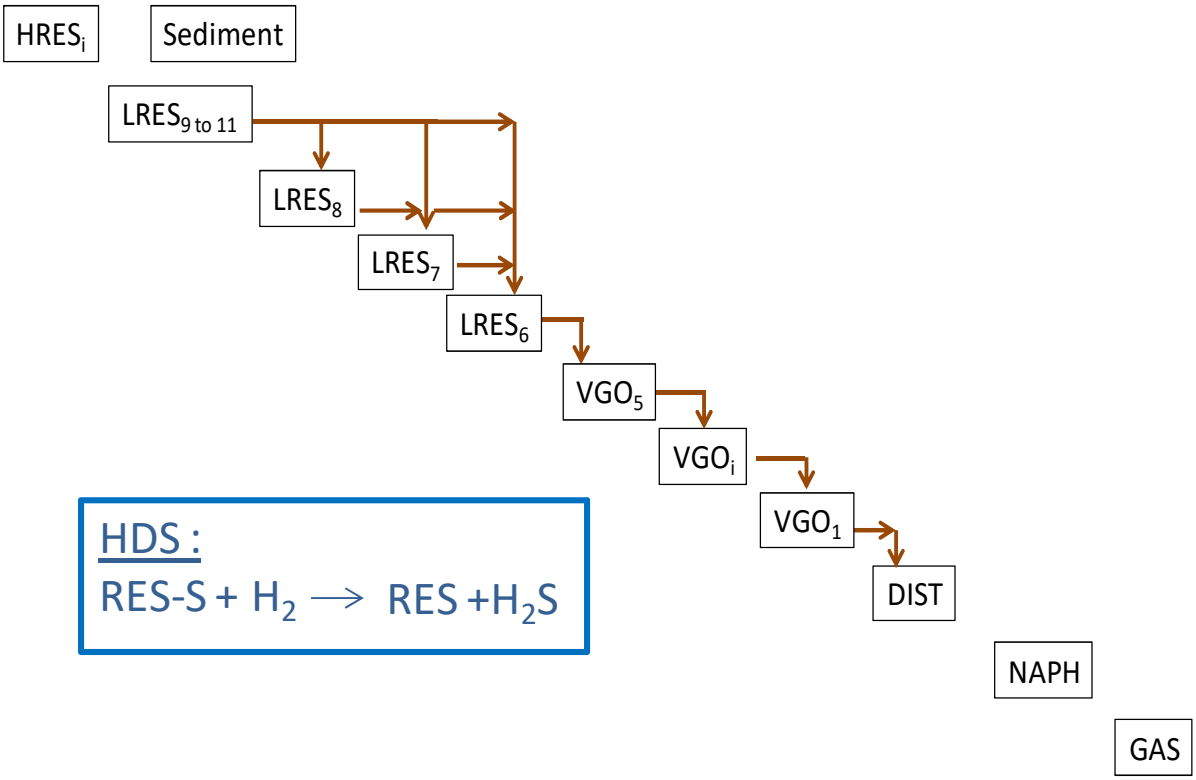

Figure 8. Reaction scheme for catalytic reaction set 4 and HDS

Reactions 4 and HDS are defined as catalytic and shown in Figure 8 and listed in Eq.s (22) to (25). Reaction 4 is a cascade through the LRES, VGO and DIST with the lighter lumps from $LRES_7$ having a single product. Material generated from the heavier lumps, $LRES_8$ to $LRES_{11}$, is divided evenly between its products. So, no stoichiometric coefficient or repartition parameter is required. As the available sulphur content data is global, we assume that the HDS reaction consumes sulphur from the RES lump and produces H_2S.

Reaction 4: (22)

$$LRES_i + \nu_{H_2} H_2 \rightarrow \nu_{3_i} LRES_j$$

with i from 7 to 11 and j from 6 to 8

$$LRES_1 + \nu_{H_2} H_2 \rightarrow \nu_{3_i} VGO_5 \quad (23)$$

$$VGO_i + \nu_{H_2} H_2 \rightarrow \nu_{3_i} VGO_{i-1} \quad (24)$$

HDS reaction:

$$RES\_S_i + H_2 \rightarrow RES_i + H_2S \quad (25)$$

Component disappearance rates are given by Eq.s (26) to (28). The Arrhenius equation is written using natural logs because we estimate the $ln(k_{0,r})$ values to reduce correlation between the parameters (see section 3.3).

$$r_{r,i} = \nu_{r,i} k_r C_i^n \qquad \text{with } r = 1, 2, \text{ and } 3 \quad (26)$$

$$r_{r,i} = \nu_{r,i} k_r C_i^n C_{H_2} \text{ with r= 4 and HDS} \quad (27)$$

$$ln(k_r) = ln(k_{0,r}) - \frac{Ea_r}{RT} \quad (28)$$

Reactions 4 and HDS are first order with respect to H_2 concentration. Reaction set 4 is also first order with respect to hydrocarbons whilst the HDS reaction order is 4 for the sulphur concentration. The H_2 consumption rate is assumed linearly dependent on only reaction temperature and global reaction rate. It requires two parameters as shown in Eq. (29), where η_1 applies to $Tref$.

$$v_{H_2} = \eta_1 + \eta_2 . (T - T_{ref})$$

(29)

For the lumps undergoing reactions 1 and 2, a linear function is used to represent the reaction orders as shown in Eq. (30), where *i* corresponds to the lumps VGO_1 to $LRES_{11}$

$$n = n_1 i + n_2 \quad (30)$$

$$k_{0,r,i} = k_{0,r} \exp(f . i) \quad (31)$$

Finally, as shown in Eq. (31) a parameter is incorporated into the pre-exponential reaction constant to provide a reactivity distribution for lumps, *i*, VGO_1 to $LRES_{11}$ undergoing reactions 1 and 2. This reactivity parameter, *f*, compensates the effect of the reaction order distribution on lump reaction rates and allows them to increase with boiling point as observed in the literature [44].

3.3. Parameter estimation

There are 18 parameters estimated for a total of 1440 data points using the MATLAB non-linear least squares solver function, lsqnonlin, with the trust-region-reflective algorithm. This minimises an objective function based on an input vector of differences between the measured and calculated data. The parameters are listed in Table 1. There are no stoichiometric coefficients estimated for reaction sets 3, 4 or HDS and the VGO product repartition parameter applies only to reaction set 1. The data points are from the online GC mass flow rate analysis for the outlet gas stream and the HTSD analysis, lumped according to the method described in section 3.2 Kinetic model and reported in mass units.

	Reactions				
Reaction specific parameters:	1	2	3	4	HDS
Pre-exponential constants	$\ln(k_1)$	$\ln(k_2)$	$\ln(k_3)$	$\ln(k_4)$	$\ln(k_{HDS})$
Activation energies	Ea_1	Ea_2	Ea_3	Ea_4	Ea_{HDS}
Stoichiometric coefficients	ν_1	ν_2			
VGO product repartition	α				
General parameters:					
Reaction order	n_1	n_2			
Reactivity parameter	f				
H_2 consumption coefficients	η_1	η_2			

Table 1. Parameters for estimation

Parameter significance levels and confidence limits are determined from the standard calculation method assuming that errors in the data are normally distributed and bearing in mind the nonlinearity of this model. The lsqnonlin Jacobian output matrix, *J*, is used to find the standard error, $se(b_p)$, from Eq.s (32) to (33) with *SSE*, *n* and *p* the sum of the errors squared and the numbers of data points and parameters respectively. The standard error is then input to Eq. (34) to find an observed value of *t* and hence the statistical significance of each parameter. Eq. (35) is used to calculate the confidence limits.

$$H = J^T J \tag{32}$$

$$se(b_p) = \sqrt{\frac{SSE\ (H^T)_{pp}}{(n_d - p)}} \tag{33}$$

$$\mathrm{t}_{obs} = \frac{b_p}{se(b_p)} \tag{34}$$

$$b_p \pm\ se(b_p)\mathrm{t}(n_d - p; \alpha_\mathrm{t}/2) \tag{35}$$

4. Results and Discussion

Table 2 gives the estimated parameters and corresponding 95% confidence limits. As stated in section 3.2 Kinetic model, the reaction constants are estimated in the form of natural logs, ln(k_0). However, the reported values are the natural logs of the reaction constants at the reference temperature ln(k_{Tref}). All the parameters are significant to 95% and the sum of errors squared can be broken down into totals for the hydrocarbons and gases, respectively, as 0.064 g^2 and 1.72 $g^2.s^{-2}$. The confidence limits are acceptable, although quite wide for the catalytic reaction sets; 4 and HDS. Nine of the parameters estimated apply to reaction set 1 and, so, as might be expected, there is some correlation and this is a potential area for model improvement. The product from reaction set 1 is distributed linearly amongst the VGO lumps. The negative estimated value for η_2 demonstrates that the H_2 consumption rate decreases with temperature relative to the sum of the rates for all the reaction sets. In hydroconversion it is the hydrogenation reactions which are catalytic and so this is consistent with a system comprising both catalytic and thermally activated cracking reactions. The calculated activation energies for reactions 1, 2 and 3 are quite high but similar to those found in the literature for lumped models for hydroconversion of heavy residues such as in the work of Nguyen et al. [13] and Asaee et al. [14]. This can be explained by the fact that our model

considers a distributed reaction order. If a first-order reaction is assumed for all the lumps, as in the case of other distributed kinetic models [19, 21-26], lower values would be obtained. The results for n_1 and n_2 correspond to an order on the hydrocarbon lump for reaction sets 1 and 2 which is 1.5 times greater for VGO_1 than for RES_6. Also, the value of the VGO product repartition parameter, α, indicates that reaction set 1 produces 1.78 times more VGO_1 than VGO_5. These two results are in accordance with one another since the lighter the lump, the greater the number of products received and increased reaction order represents more heterogeneity in the reactivity of the lumped species.

Stangeland's model [19] has applied a first order reaction for a boiling range which vary between 200 to 500°C. The boiling range in this work (100 to 980 °C) is wider than that of Stangeland. The kinetic constants of this work depend on the reaction order and the reactivities can't be compared directly with Stangeland those. Note that one of the wide range of models including only first order reaction has been tested but it was unable to fit our data.

Reaction specific parameters

Reaction	$\ln(k_{Tref})$ $(mol^{-1}.m^3)^{n-1}.s^{-1}$	Ea $(kJ.mol^{-1})$	v (-)	α (-)
1	-22.7 ± 0.9	289 ± 4	5.14 ± 0.07	0.028 ± 0.012
2	-23.5 ± 1.7	334 ± 10	2.65 ± 0.38	
3	-8.36 ± 0.5	306 ± 3		
4	-16.8 ± 2.6*	76.3 ± 15.3		
HDS	-36.8 ± 2.0*	147 ± 12		

*$(mol^{-1}.m^3)^n.s^{-1}$

General parameters

n_1	n_2	f	η_1	η_2
-0.106 ± 0.020	3.22 ± 0.14	0.845 ± 0.071	0.988 ± 0.046	-0.264 ± 0.030

Table 2. Estimated parameters with reaction constants adjusted to those for T_{ref}

Figure 9 confirms that the residuals are mostly uniform and centered around zero. The data is in mass units and the measurement error increases with quantity, so the largest errors are for the components in the greatest amounts. The errors for the gases are less well centred in the mass balance data which could be related to the equilibrium calculations. The largest error ranges were obtained for lumps with the largest boiling point ranges, NAPH and DIST. This result shows that a more detailed description of lumps by smaller temperature ranges allows higher precision to be achieved.

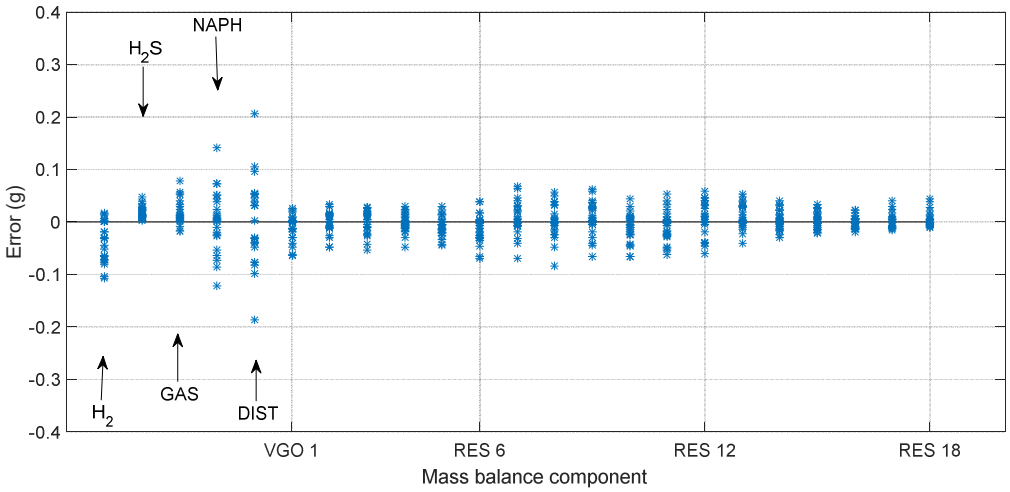

Figure 9. Errors for components and lumps after parameter estimation (measured data minus simulated values)

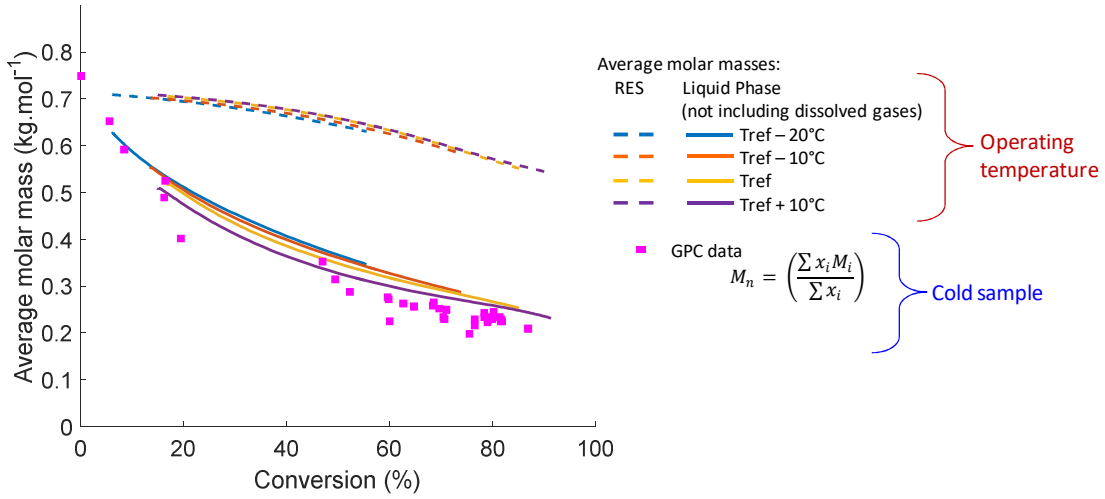

Figure 10. Average molar masses at different conversions: calculated values for liquid phase hydrocarbons (solid lines) and residue (dotted lines) and measured by GPC for a similar set of experiments

Figure 10 shows calculated and measured values of average RES and liquid phase molar mass for all the experiments. As would be expected, the RES average molar mass is greater than that of all the liquid phase hydrocarbons. The results demonstrate the evolution of the RES molar mass with processing. The lumping strategy therefore allows the model to represent the changes in average molar mass and volume with sufficient precision. This confirms the utility of the lumping method for the physical property calculations. Note that the GPC analysis results are for the reactor contents after cooling and are therefore not directly comparable with the calculated values, which are for the reactor liquid phase during operation. This explains the difference above 60% conversion, since volatiles which are found in the reactor vapour phase during operation are condensed on cooling and therefore only present in the GPC analysis.

Figure 11 and Figure 12 give an example of the model outputs for T_{ref}. Figure 11 compares the calculated quantities of the reaction components to the measured data, as well as the mass

flow rates of the outlet gases. The mass balance data and mass flow rates are given relative to the initial mass of RES and the incoming H_2 mass flow rate respectively. We can observe that, at this temperature, the model fits the initial rapid decay in the RES quantity and the concomitant increases in all the products. The model also reproduces the behaviour of the VGO, which is quite static and only begins to decrease at high conversion whilst the NAPH, GAS and H_2S all accumulate slowly. Figure 11 (b) shows that the experimental delay in the outlet gas mass flow reaching the analyser is well represented. Also, that the model computes the sudden release of GAS and H_2S at the start of the operation correctly followed by their steady decay.

Figure 12 compares the measured and calculated masses of the RES_i and VGO_i lumps for T_{ref} at different reaction times and clearly displays how the calculated composition of this boiling range follows its measured evolution.

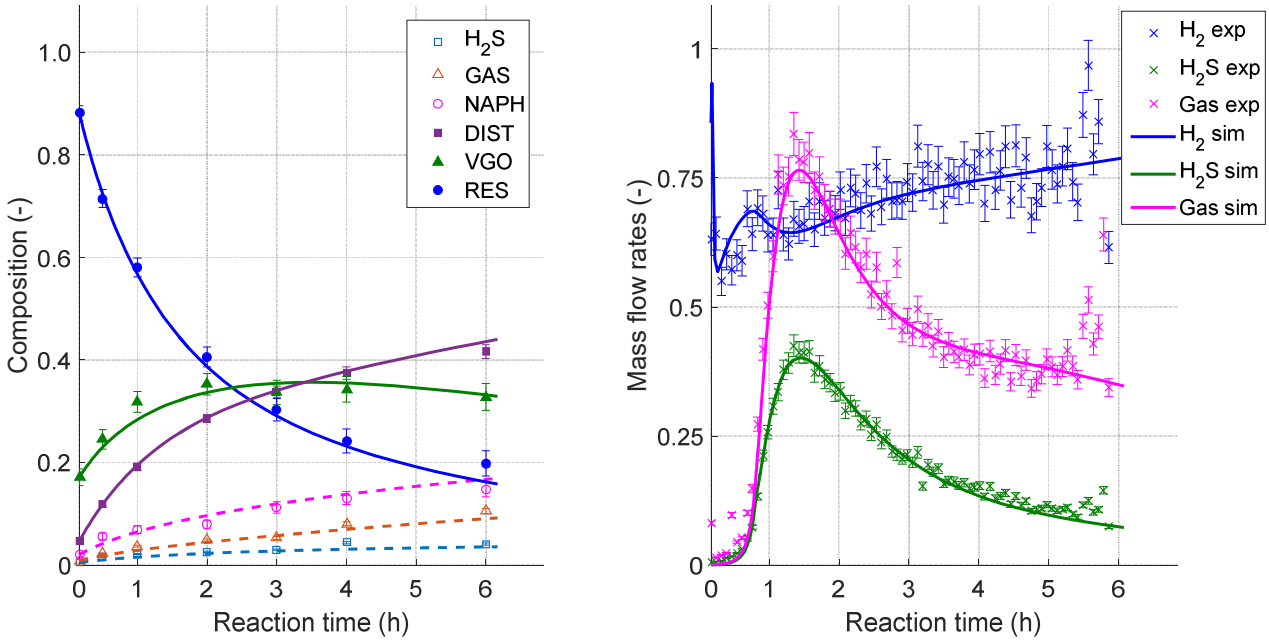

(a) (b)

Figure 11. Model outputs and experimental data for T_{ref} (a) reactor quantities per mass unit of RES introduced to the reactor (b) outlet gas mass flow rates per unit of H_2 entering the system

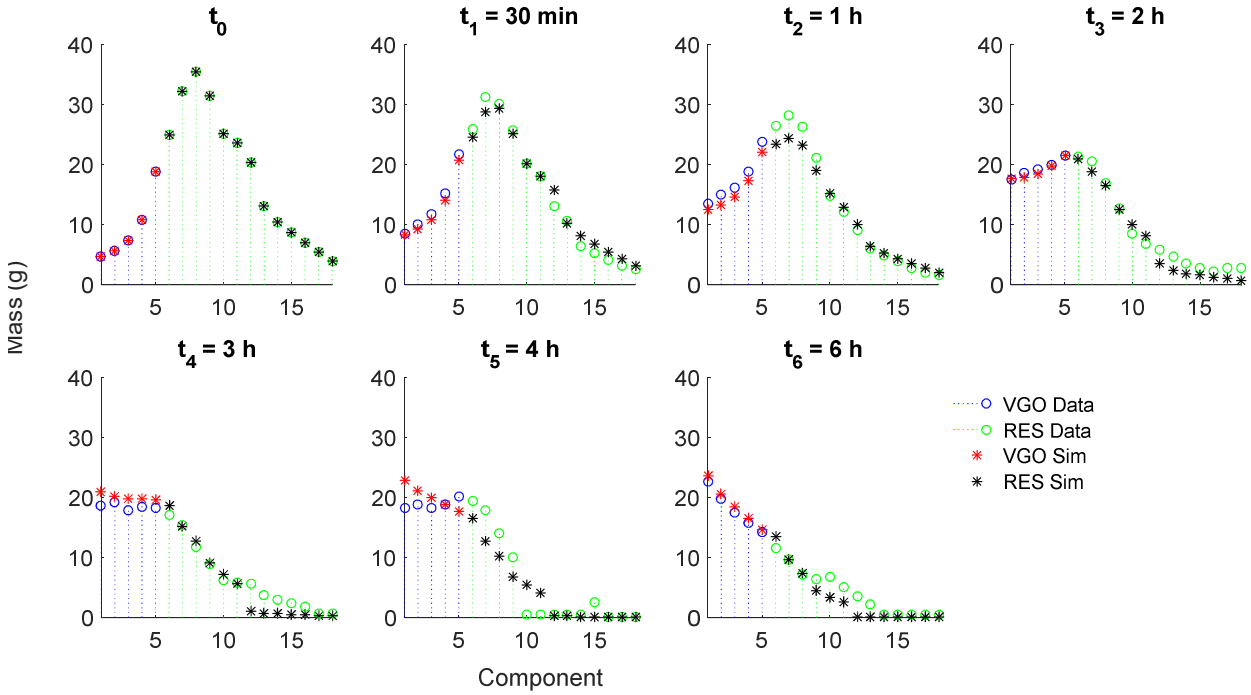

Figure 12. Comparison of measured and calculated masses of VGO_i and RES_i lumps for T_{ref} at different reaction times

Figure 13, Figure 14 and Figure 15 give parity plots for the results at all the experimental temperatures. Figure 13 gives the parity plot for all the RES_i and VGO_i lumps and for all 28 experiments including ± 10% lines (here, the parity line represents the same information as the x-axis in Figure 9). Figure 14 shows the detail for the mass balance components and Figure 15 reports the result for the online gas GC data. In general, the parity plots show a good fit between the calculated and measured data.

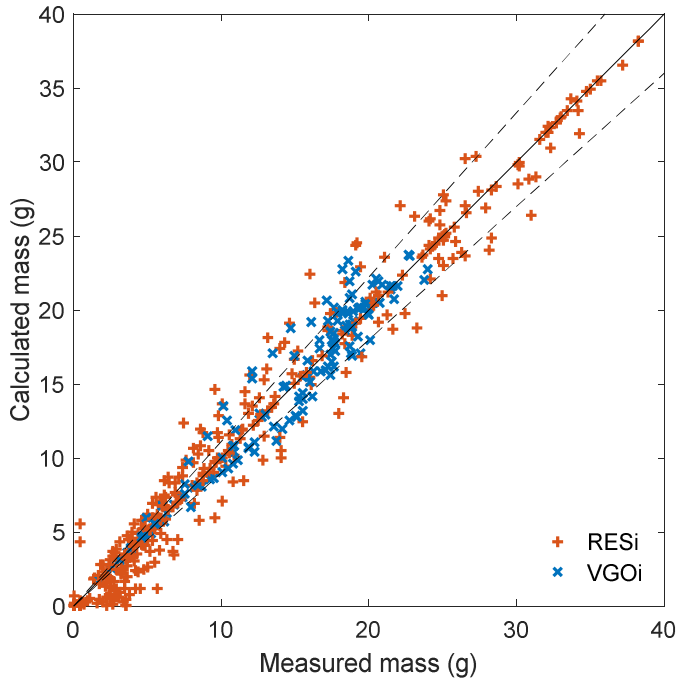

Figure 13. Parity plot for calculated masses of all RES_i and VGO_i lumps against mass balance data including ± 10% lines.

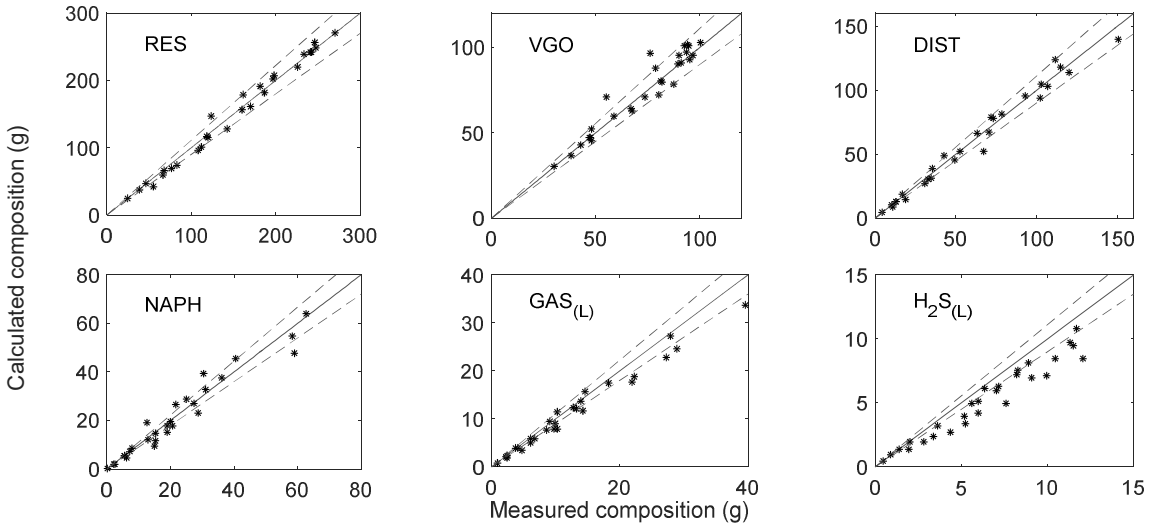

Figure 14. Parity plots for calculated masses of components and refinery cuts against mass balance data including ± 10% lines.

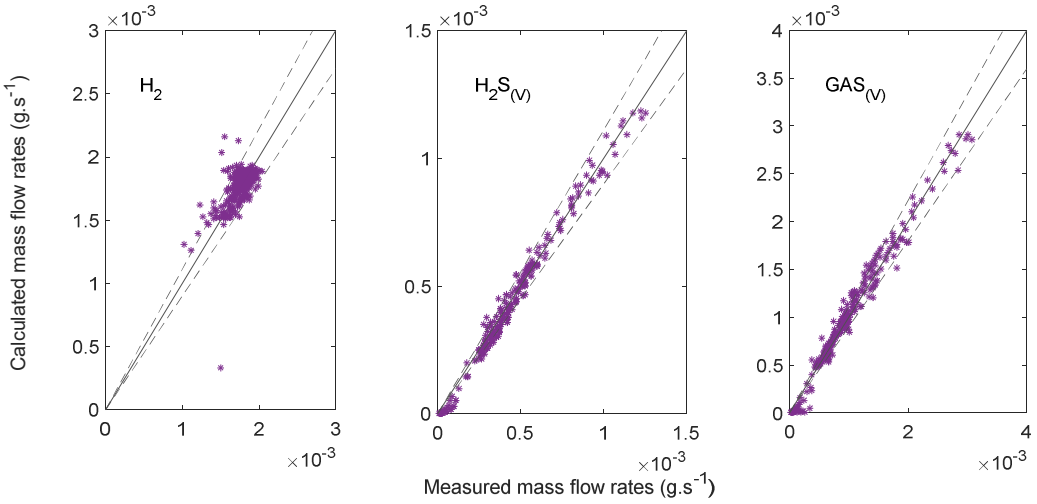

Figure 15. Parity plots for calculated gas mass flow rates against measured data including ± 10% lines.

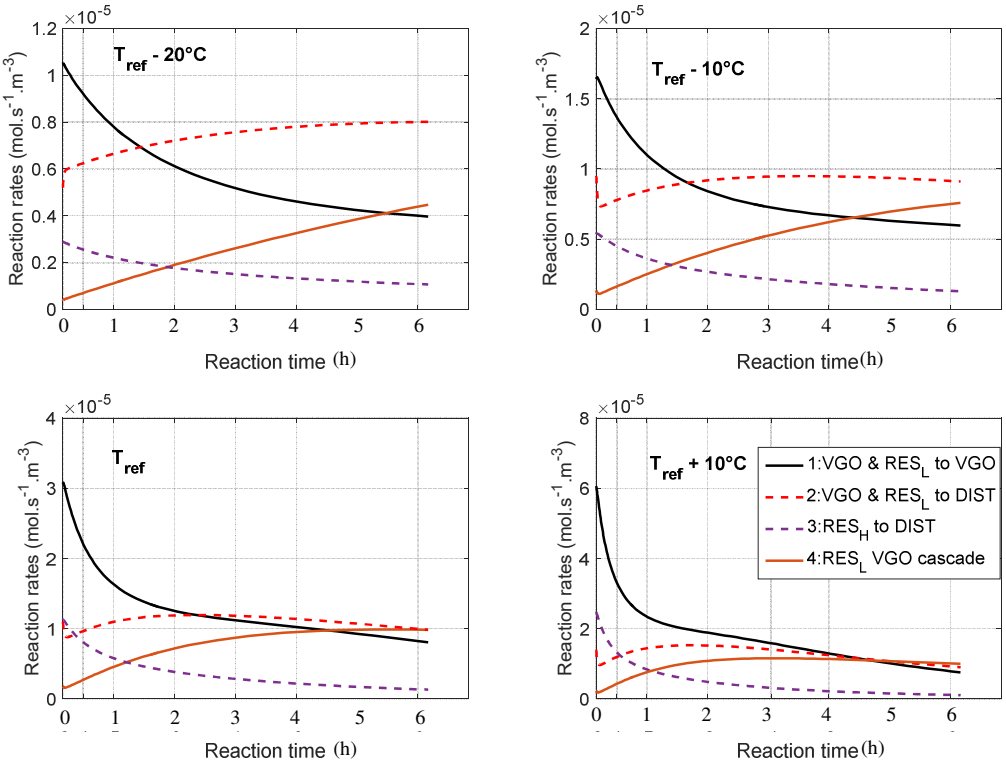

Figure 16. Calculated reaction rates at different operating temperatures

Figure 16 compares the reaction rates at each operating temperature. We can see that reactions 1 and 2 are dominant at low conversion, earlier in the reaction period. They both have high activation energies (see Table 2) which confirms they are thermally activated. Reaction 3 breaks down heavy residue boiling at 735°C+ into DIST by a first order reaction. The sediment, formed as secondary product in this reaction was not detected by the analysis but was visible to the eye. Reaction 4 has more impact at higher conversion, later in the reaction period. The low estimated value of its activation energy verifies that this cascade through the VGO and RES cuts, is catalytic. The fact that this reaction can be represented as first order reaction suggests a similar mechanism for all the molecular structures present.

5. Conclusions

Classical models are not yet sufficient to accurately represent the evolution of RES physical properties during hydroconversion. The use of distributed lumps for the VGO and RES cuts allows this variation to be represented and reaction rate equations based on molar concentrations can be used. Without this adaptation correlations are needed to estimate the molar masses and volumes at different conversions. So, this method provides a real step forward in the modelling technique for this type of system. The combination of GPC and simulated distillation analysis results also validated the extrapolation of the heavy fluids composition to the whole VR boiling range. This is required to initialise the distributed lump model and is also of benefit for the parameter estimation as it provides more data. Finally, the proposed model and reaction scheme enabled us to obtain a good fit with the measured data for a reasonable number of parameters.

Acknowledgements

The authors would like thank IRCELYON for experimental analysis and TOTAL for the financial support.

Nomenclature

a,b,d	Parameters for HTSD extrapolation (-)
b_p	Parameter value (-)
A,B	Parameters for Riazi extrapolation method [43] (-)
C	Concentration ($mol.m^{-3}$)
Ea	Activation energy ($kJ.mol^{-1}$)
f	Reactivity parameter (-)
H	Matrix for confidence limit calculation
k	Reaction constant
k_la	Vapour –liquid mass transfer coefficient
M	Molar mass ($g.mol^{-1}$)
n	Quantity (mol)
$\dot{n}$	Flow rate ($mol.s^{-1}$)
n	Reaction order (-)
n_d	Number of data points
J	Jacobian matrix
N_{VGO}	Number of VGO lumps
p	Number of parameters
r	Reaction rate ($mol.s^{-1}.m^{-3}$)
R	Ideal gas constant ($kJ.mol^{-1}.K^{-1}$)
t	Time (s)
t	Student's t-distribution (-)
T	Temperature (K)
T_b	Boiling point (K)
T_{b0}	Initial boiling point (K)
V	Volume (m^3)

V_{mol}	Molar volume (mol.m^{-3})
x_c	Distilled fraction (-)
x_{i_reflux}	Mole fraction condensed (-)
y	Vapour mole fraction (-)
α	Parameter for repartition coefficient for reaction 1VGO product (-)
α_t	Confidence level for the student's t-distribution (-)
β	Repartition coefficient for reaction 1VGO product (-)
η_1, η_2	H_2 consumption rate parameters (-), (K^{-1})
v	Stoichiometric coefficient (-)

Subscripts/superscripts

c	Condenser
ech	Exchange between liquid and vapour phase
H₂_supply	Stream identification for H_2 supply
hot_gas	Stream identification for hot gases leaving the reactor
i,j	Lump
L	Liquid phase
op	Operating
prod	Production
r	Reaction
R	Reactor
reflux	Reflux from condenser to reactor
V	Vapour phase

References

[1] O. Publishing, World Energy Outlook 2017, OECD Publishing, Paris, 2017. http://public.eblib.com/choice/PublicFullRecord.aspx?p=5160837 (accessed March 19, 2018).
[2] A. Shah, R. Fishwick, J. Wood, G. Leeke, S. Rigby, M. Greaves, A review of novel techniques for heavy oil and bitumen extraction and upgrading, Energy Environ. Sci. 3 (2010) 700. doi:10.1039/b918960b.
[3] R. Sahu, B.J. Song, J.S. Im, Y.-P. Jeon, C.W. Lee, A review of recent advances in catalytic hydrocracking of heavy residues, J. Ind. Eng. Chem. 27 (2015) 12–24. doi:10.1016/j.jiec.2015.01.011.
[4] L.C. Castañeda, J.A.D. Muñoz, J. Ancheyta, Combined process schemes for upgrading of heavy petroleum, Fuel. 100 (2012) 110–127. doi:10.1016/j.fuel.2012.02.022.
[5] J. Weitkamp, Catalytic Hydrocracking—Mechanisms and Versatility of the Process, ChemCatChem. 4 (2012) 292–306. doi:10.1002/cctc.201100315.
[6] J.G. Speight, New approaches to hydroprocessing, Catal. Today. 98 (2004) 55–60. doi:10.1016/j.cattod.2004.07.053.
[7] T. Cordero-Lanzac, I. Hita, A. Veloso, J.M. Arandes, J. Rodríguez-Mirasol, J. Bilbao, T. Cordero, P. Castaño, Characterization and controlled combustion of carbonaceous deactivating species deposited on an activated carbon-based catalyst, Chem. Eng. J. 327 (2017) 454–464. doi:10.1016/j.cej.2017.06.077.
[8] S. Zhang, D. Liu, W. Deng, G. Que, A Review of Slurry-Phase Hydrocracking Heavy Oil Technology, Energy Fuels. 21 (2007) 3057–3062. doi:10.1021/ef700253f.
[9] C.J. Calderón, J. Ancheyta, Modeling of Slurry-Phase Reactors for Hydrocracking of Heavy Oils, Energy Fuels. 30 (2016) 2525–2543. doi:10.1021/acs.energyfuels.5b02807.
[10] A. Quitian, J. Ancheyta, Experimental Methods for Developing Kinetic Models for Hydrocracking Reactions with Slurry-Phase Catalyst Using Batch Reactors, Energy Fuels. 30 (2016) 4419–4437. doi:10.1021/acs.energyfuels.5b01953.
[11] M.M. Carbonell, R. Guirardello, Modelling of a slurry bubble column reactor applied to the hydroconversion of heavy oils, Chem. Eng. Sci. 52 (1997) 4179–4185. doi:10.1016/S0009-2509(97)88933-6.
[12] J.F. Mosby, R.D. Buttke, J.A. Cox, C. Nikolaides, Process characterization of expanded-bed reactors in series, Chem. Eng. Sci. 41 (1986) 989–995. doi:10.1016/0009-2509(86)87184-6.
[13] T.S. Nguyen, M. Tayakout-Fayolle, M. Ropars, C. Geantet, Hydroconversion of an atmospheric residue with a dispersed catalyst in a batch reactor: Kinetic modeling including vapor–liquid equilibrium, Chem. Eng. Sci. 94 (2013) 214–223. doi:10.1016/j.ces.2013.02.036.
[14] S.D.S. Asaee, L. Vafajoo, F. Khorasheh, A new approach to estimate parameters of a lumped kinetic model for hydroconversion of heavy residue, Fuel. 134 (2014) 343–353. doi:10.1016/j.fuel.2014.05.079.
[15] C.J. Calderón, J. Ancheyta, Modeling of CSTR and SPR small-scale isothermal reactors for heavy oil hydrocracking and hydrotreating, Fuel. 216 (2018) 852–860. doi:10.1016/j.fuel.2017.11.089.
[16] F. Alhumaidan, H. Lababidi, H. Al-Adwani, Hydrocracking of atmospheric residue feedstock in hydrotreating processes, Kuwait J. Sci. Eng. (2010) 129–159.
[17] Z. Till, T. Varga, L. Szabó, T. Chován, Identification and Observability of Lumped Kinetic Models for Vacuum Gas Oil Hydrocracking, Energy Fuels. 31 (2017) 12654–12664. doi:10.1021/acs.energyfuels.7b02040.
[18] R.I. Rueda-Velásquez, M.R. Gray, A viscosity-conversion model for thermal cracking of heavy oils, Fuel. 197 (2017) 82–90. doi:10.1016/j.fuel.2017.02.020.

[19] B.E. Stangeland, A Kinetic Model for the Prediction of Hydrocracker Yields, Ind. Eng. Chem. Process Des. Dev. 13 (1974) 71–76. doi:10.1021/i260049a013.
[20] C.S. Laxminarasimhan, R.P. Verma, P.A. Ramachandran, Continuous lumping model for simulation of hydrocracking, AIChE J. 42 (1996) 2645–2653. doi:10.1002/aic.690420925.
[21] S. Mohanty, D.N. Saraf, D. Kunzru, Modeling of a hydrocracking reactor, Fuel Process. Technol. 29 (1991) 1–17. doi:10.1016/0378-3820(91)90013-3.
[22] M.A. Pacheco, C.G. Dassori, Hydrocracking: an improved kinetic model and reactor modeling, Chem. Eng. Comm. 189 (2002) 1684–1704. doi:10.1080/00986440290013013.
[23] G. Li, Y. Xia, W. Zeng, Kinetic mechanism research of an industrial hydrocracker based on strict calculation of stoichiometric coefficients, Fuel. 103 (2013) 285–291. doi:10.1016/j.fuel.2012.09.044.
[24] G. Li, C. Cai, Estimation parameters of hydrocracking model with NSGA-ii (Non-dominated Sorting Genetic Algorithm) by using discrete kinetic lumping model, Fuel. 200 (2017) 333-344. doi:10.1016/j.fuel.2017.03.078.
[25] H. Harode, M. Ramteke, Axial dispersion modeling of industrial hydrocracking unit and its multiobjective optimization, Chem. Eng. Res. Des. 121 (2017) 57-68. doi:10.1016/j.cherd.2017.02.033
[26] H.J. Martinez-Grimaldo, J.C. Chavarria-Hernandez, J. Ramirez, R. Cuevas, H. Ortiz-Moreno, Prediction of Sulfur Content, API Gravity, and Viscosity Using a Continuous Mixture Kinetic Model for Maya Crude Oil Hydrocracking in a Slurry-Phase Reactor, Energy Fuels. 25 (2011) 3605–3614. doi:10.1021/ef2005942.
[27] T. Jansen, D. Guerry, E. Leclerc, M. Ropars, M. Lacroix, C. Geantet, M. Tayakout-Fayolle, Simulation of Petroleum Residue Hydroconversion in a Continuous Pilot Unit Using Batch Reactor Experiments and a Cold Mock-Up, Ind. Eng. Chem. Res. 53 (2014) 15852–15861. doi:10.1021/ie502242f.
[28] J. Ancheyta, S. Sánchez, M.A. Rodríguez, Kinetic modeling of hydrocracking of heavy oil fractions: A review, Catal. Today. 109 (2005) 76–92. doi:10.1016/j.cattod.2005.08.015.
[29] G.G. Martens, G.B. Marin, Kinetics for hydrocracking based on structural classes: Model development and application, AIChE J. 47 (2001) 1607–1622. doi:10.1002/aic.690470713.
[30] H. Kumar, G.F. Froment, Mechanistic Kinetic Modeling of the Hydrocracking of Complex Feedstocks, such as Vacuum Gas Oils, Ind. Eng. Chem. Res. 46 (2007) 5881–5897. doi:10.1021/ie0704290.
[31] S.R. Horton, Z. Hou, B.M. Moreno, C.A. Bennett, M.T. Klein, Molecule-based modeling of heavy oil, Sci. China. Chem. 56 (2013) 840–847. doi:10.1007/s11426-013-4895-8.
[32] L. Zhang, Z. Hou, S.R. Horton, M.T. Klein, Q. Shi, S. Zhao, C. Xu, Molecular Representation of Petroleum Vacuum Resid, Energy Fuels. 28 (2014) 1736–1749. doi:10.1021/ef402081x.
[33] S.R. Horton, L. Zhang, Z. Hou, C.A. Bennett, M.T. Klein, S. Zhao, Molecular-Level Kinetic Modeling of Resid Pyrolysis, Ind. Eng. Chem. Res. 54 (2015) 4226–4235. doi:10.1021/ie5041572.
[34] R.I. Rueda-Velázquez, M.R. Gray, Monte Carlo Simulation of Asphaltenes and Products from Thermal Cracking, Energy Fuels. 28 (2014) 2352-2364. doi:10.1021/ef402390w.
[35] L.P. Oliveira, J.J. Verstraete, M. Kolb. Simulating vacuum residue hydroconversion by means of Monte-Carlo techniques, Catal. Today. 220-222 (2014) 208–220. doi:10.1016/j.cattod.2013.08.011.

[36] P.E. Savage, M.T. Klein, Asphaltene reaction pathways - V. Chemical and mathematical modeling. Chem. Eng. Sci. 44 (1989) 393–404. doi:10.1016/0009-2509(89)85076-6.
[37] M. Neurock, C. Libanati, A. Nigam, M.T. Klein, Monte Carlo simulation of complex reaction systems: Molecular structure and reactivity in modelling heavy oils. Chem. Eng. Sci. 45 (1990) 2083−2088. doi:10.1016/0009-2509(90)80080-X.
[38] M. Neurock, A. Nigam,. D. Trauth, M.T. Klein, Molecular representation of complex hydrocarbon feedstocks through efficient characterization and stochastic algorithms. Chem. Eng. Sci. 49 (1994) 4153−4177. doi:10.1016/S0009-2509(05)80013-2.
[39] T.T.H. Nguyen, S. Teratani, R. Tanaka, A. Endo, M. Hirao, Development of a Structure-Based Lumping Kinetic Model for Light Gas Oil Hydrodesulfurization, Energy Fuels. 31 (2017) 5673–5681. doi:10.1021/acs.energyfuels.7b00360.
[40] W. Wei, C.A. Bennett, R. Tanaka, G. Hou, M.T. Klein Jr, M.T. Klein, Computer aided kinetic modeling with KMT and KME, Fuel Process. Technol. 89 (2008) 350–363. doi:10.1016/j.fuproc.2007.11.015
[41] ASTM D7169-16, Standard Test Method for Boiling Point Distribution of Samples with Residues Such as Crude Oils and Atmospheric and Vacuum Residues by High Temperature Gas Chromatography, (2016). www.astm.org.
[42] A. Vickers, Higher-Temperature Simulated Distillation with DB-HT Sim Dis Columns: Application, Hydrocarbon Processing, (2002). https://www.agilent.com/cs/library/applications/5988-7929EN.pdf (accessed March 12, 2018).
[43] M.R. Riazi, Characterization and properties of petroleum fractions, ASTM International, W. Conshohocken, PA, 2005.
[44] J. Weitkamp, The Influence of Chain Length in Hydrocracking and Hydroisomerization of *n* -Alkanes, in: J.W. Ward, S.A. Qader (Eds.), Hydrocracking Hydrotreating, AMERICAN CHEMICAL SOCIETY, WASHINGTON, D. C., 1975: pp. 1–27. doi:10.1021/bk-1975-0020.ch001.

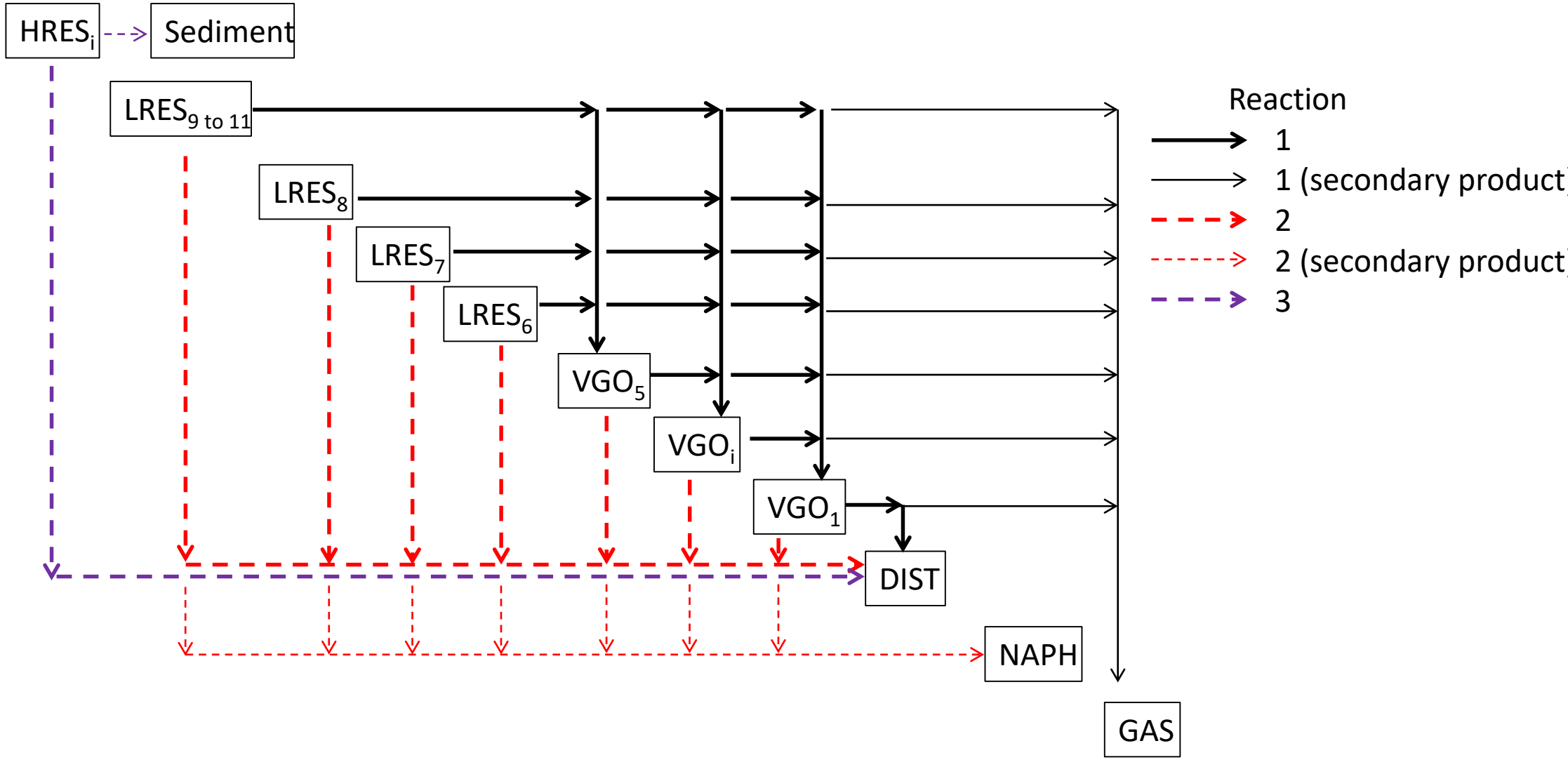
HRES$_i$
Sediment
LRES$_{9\ to\ 11}$
LRES$_8$
LRES$_7$
LRES$_6$
VGO$_5$
VGO$_i$
VGO$_1$
DIST
NAPH
GAS
Reaction
1
1 (secondary product)
2
2 (secondary product)
3